

Hyaluronic Acid/Alginate Hydrogel Permeability

Vidhi Maheshwari, PhD; Daniel L. Peterson, MD; Sarah M. Mayes, PhD

Alafair Biosciences Inc., Austin, TX

Abstract: Nerve cuffs are implant devices designed to provide a protecting interface between peripheral nerve and surrounding tissues. This interface physically isolates damaged nerve tissue from unwanted excessive injury response, while preserving the delicate microenvironment required to heal nerve. An important attribute of successful nerve cuffs is selective and timely permeability, allowing desired macromolecules to reach the healing tissue while discouraging unwanted scar formation that can inhibit optimal outcomes. A permeability study using a diverse range of molecular weight dextrans determined that a hyaluronic acid (HA) and alginate (Alg)-based hydrogel is nano-porous, easily permeable to macromolecules with Stokes radius up to 3.6 nm within six (6) hours and to 7 nm over longer time periods. Migration of biomolecules and growth factors occurs via passive diffusion; available polyanionic carboxylate groups immobilize a relatively large volume of water within the hydrogel, facilitating rapid exchange of oxygen and nutrients. The HA/Alg hydrogel is bioresorbed via layer-by-layer degradation over a 2-year period, providing an increasingly permeable interface as healing progresses. This selective and timely permeability provides an ideal encasement of healing nerve by preserving a desired microenvironment of growth factors and nutrients and by reducing initial infiltration of large scar tissue forming fibroblasts.

INTRODUCTION

Peripheral nerve repair and regeneration remains a significant challenge for tissue engineering and regenerative medicine. Peripheral nerves have an extraordinary yet limited capacity to regenerate after an injury; thus, peripheral nerve injuries with incomplete functional and sensory recovery can be particularly incapacitating for patients [1, 2]. The pathophysiology of nerve injury and repair is a complex process that depends on the interaction of the nerve cell body, the axonal fiber, and the surrounding milieu (**Fig 1**). Within 20 minutes to 6 hours, initial homeostatic response is essentially mediated by calcium influx resulting in calpain increase that triggers axonal degeneration [3], growth cone formation, and histiocytic cell activation with migration of macrophages to the region of damage [4] to facilitate phagocytosis of debris [5]. In addition to a phagocytic role, macrophages secrete substances that aid in Schwann Cell (SC's) proliferation near axon lesions as well as mitogens, nerve growth factor (NGF), insulin-like growth factor (IGF), platelet-derived growth factor (PDGF), and apolipoprotein-E that are important in axonal elongation and remyelination [6, 7]. SC's physically guide axons to target tissues and secrete extracellular proteins that promote axonal extension [4]. Ultimately, proliferative SCs undergo dedifferentiation and transform their phenotype to ensheath and myelinate immature axons [8, 9]. Macrophages also secrete multiple cytokines and chemokines that cause a pro-inflammatory response [10]. If this proinflammatory reaction is excessive or prolonged, there is an unreasonable accumulation of scar-associated molecules, such as chondroitin sulfate proteoglycans (CSPGs), which impede axonal elongation and neurite outgrowth [11]. Thus, the regulation of inflammation is crucial for axonal regeneration and remyelination following nerve trauma.

This natural response provides a microenvironment of growth factors, hormones, cytokines, and extracellular matrix (ECM) factors specific to and ideal for the injury sustained. Nerve cuffs are intended to protect this environment to produce optimal patient outcomes. A nerve cuff encases a nerve for aid in repairing the nerve (e.g., to prevent ingrowth of scar tissue) and caps the end of the nerve to prevent the formation of neuroma (tumors) [12]. For proper healing of the nerve tissue, a nerve cuff should retain the naturally released nerve growth factors secreted by the damaged nerve stumps, and simultaneously reduce the invasion of scar tissue-forming fibroblasts to the injury site [1].

Hyaluronic acid (HA) and alginate (Alg) are widely used hydrophilic biopolymers known for their anti-adhesive and wound healing properties [13-17]. Alginate and HA-based hydrogels have been extensively investigated for the repair of the central and peripheral nerve systems. Alginate-based highly anisotropic capillary gels introduced into acute cervical spinal cord lesions in adult rats were integrated into the spinal cord parenchyma without major inflammatory responses and supported direction of axonal regrowth [18]. Cross-linked alginate hydrogels were useful to restore a 50-mm gap in feline sciatic nerves [19], and promoted the outgrowth of regenerating axons and astrocyte reactions at the stump of transected spinal cords in young rats [20]. Alginate-based hydrogels were applied as glue for repair of peripheral nerve gaps that could not be sutured [21], and were investigated for cell-based neural therapies, as mouse-derived neural stem cells cultured in calcium alginate beads maintained their capacity for multilineage differentiation into neurons and glial cells [22].

HA is widely present in most organs and tissues [23, 24], especially in the CNS [25]; owing to its high biocompatibility, HA is an attractive biomaterial for designing and fabricating scaffolds for nerve repair and regeneration. Recent studies demonstrated that implantation of HA scaffolds reduces glial scar formation [26, 27]. Coating nerve tissues after neurolysis with HA is found to be

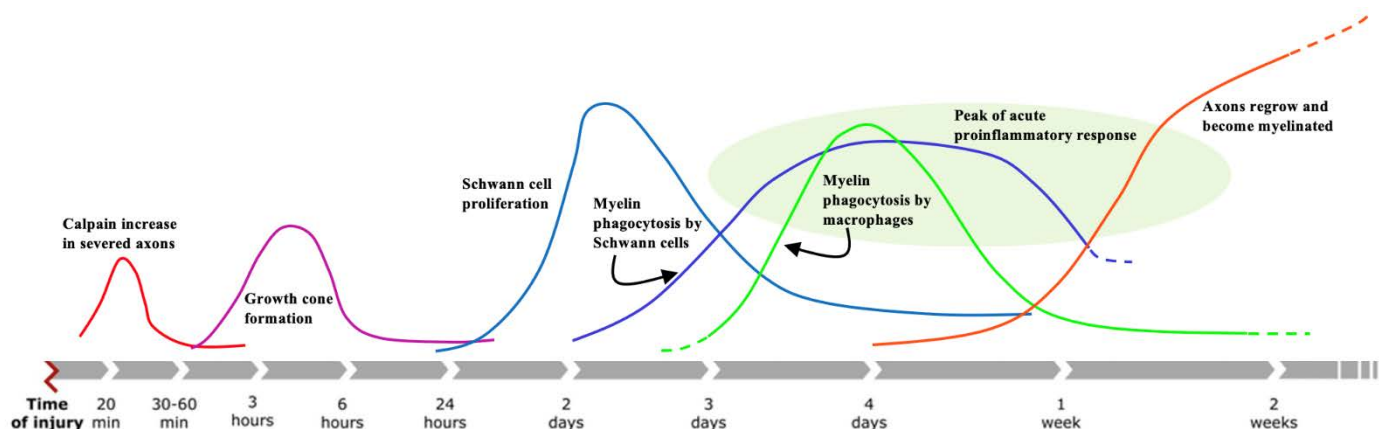


Fig 1. Timeline of major events important for nerve repair after injury (Adapted from [3])

the most effective method of reducing extra neural and intraneural scarring [28, 29]. HA has been shown to enhance peripheral nerve regeneration in a rat sciatic nerve model [30]. Seckel et. al. demonstrated that sequential delivery of HA and neurotrophic/growth factors to a regenerating rat sciatic nerve resulted in reinnervation with better conduction velocity, higher axon counts, and a trend toward earlier myelination when compared with saline treated group [31].

Medical devices consisting of HA and/or Alg include adhesion barriers, wound dressings, drug delivery hydrogels, and soft tissue protectors such as peripheral nerve cuffs [13, 28, 29, 32-38]. The present study discusses the selective permeability and surface morphology of an HA/Alg hydrogel intended to protect the microenvironment of healing, intact peripheral nerve.

MATERIALS

Technical grade dextrans ranging from 6-250 KDa were obtained from Alfa Aesar. Dextran standards ranging from 1-150 KDa were obtained from Sigma Aldrich. HA/Alg hydrogels were obtained from Alafair Biosciences. All other chemicals and reagents were of the highest purity grade commercially available.

Preparation of specimens (HA/Alg Hydrogel)

For confocal microscopy preparation, the HA/Alg hydrogels were labeled with 0.2% alginate-fluorescein and 0.75% HA-rhodamine. Specimens were covered in aluminum foil for light protection.

Dextran challenge solution (DCS)

A dextran challenge solution (DCS, 12 mL) was prepared using equal volumes (2 mL) of stock solutions of technical grade dextran (5 mg/mL) (Table 1). All stock solutions were prepared using HPLC grade water (Fisher Scientific #W5-1). DCS was syringe filtered through a 0.22 µm Millex GV Durapore PVDF membrane into a 20 mL scintillation vial.

Table 1. Technical grade dextrans comprising the challenge solution

Product #	Supplier	MW (kDa)
J62775	Alfa Aesar	6
J61216	Alfa Aesar	20
J63690	Alfa Aesar	40
J60989	Alfa Aesar	75
J63789	Alfa Aesar	150
J60200	Alfa Aesar	250

Dextran gel permeation chromatography (GPC) standards

Each gel permeation chromatography GPC standard (1 mL) was prepared using HPLC grade water at a concentration of 5 mg/mL (Table 2).

Table 2. Dextran standards for calibrating the GPC

Product #	Supplier	Nominal MW (kDa)	M _p (Da)*	PD*
31416-100MG	Sigma-Aldrich	1	1080	1.26
31417-100MG	Sigma-Aldrich	5	4440	1.60
31419-100MG	Sigma-Aldrich	25	21400	1.30
31421-100MG	Sigma-Aldrich	80	66700	1.46
31422-100MG	Sigma-Aldrich	150	123600	1.47

* The polydispersity (PD) and peak molecular weights (M_p) were obtained from the certificates of analysis.

METHODS

Scanning Electron Microscopy (SEM)

Specimens were mounted on an aluminum stub with carbon tape. The mounted specimens were coated with 10 nm of Pt/Pd via a Cressington 208 benchtop sputter coater just prior to imaging. The specimens were imaged using the Zeiss Supra 40V scanning electron microscope's secondary electron detector and a voltage of 5 kV. The top and bottom surfaces and the cross-section region of the specimens were imaged.

Confocal Microscopy

The test specimens were imaged using a Zeiss LSM710 laser scanning confocal microscope under a 60x objective for z-stacking

20 microns, or the full thickness of the specimen, whichever was smallest.

Franz Diffusion Cell

The permeation study was conducted using a PermeGear 9-station Franz cell stirrer, consisting of a receptor chamber (ID = 9 mm) filled with 5 mL of HPLC grade water, a donor chamber filled with the DCS and a diffusion barrier - specimen (equivalent to 0.64 cm² of exposed hydrogel) (Fig 2). The donor compartment and the sampling port were closed using parafilm. The receptor chamber consisted of a water jacket to maintain a constant temperature (37 °C) and a magnetic stirrer to maintain a homogenous concentration. Five (5) hydrogels were prepared this way.

After equilibrating the specimen at 25 °C for 15 mins, 0.5 mL of DCS was added to each donor compartment. The fluid in the donor compartment was transferred to a 2.0 mL microfuge tube at time points of 1.5, 6 and 24 hrs and refrigerated at 4°C until analysis.

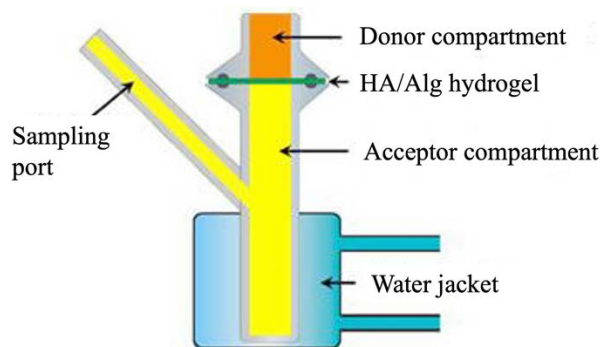


Fig 2. Experimental setup for dextran permeation through HA/Alg hydrogel using a Franz diffusion cell

Gel permeation chromatography (GPC)

A gel permeation chromatography (GPC) instrument was equipped with a differential refractometer detector, a guard column and three fractionating columns (Table 3) packed with poly(hydroxyethylmethacrylate) arranged in series. The loop volume was 20 µL. A baseline chromatogram was obtained using HPLC grade water as blank and the mobile phase. Samples were syringe filtered prior to injecting into the column. All experiments were conducted at ambient temperature, 25 °C. A flowrate of 1 mL/min was maintained at 1388 psi for 40 minutes.

Table 3. GPC columns

Column	Make	Size (mm)	Product #
Guard	Viscotek AGuard	50 x 6.0	G209501
Column 1	Viscotek A5000	300 x 8.0	L1330065
Column 2	Viscotek A3000	300 x 8.0	L210541
Column 3	Viscotek A2500	300 x 8.0	L210502

Data Analysis

A best-fit exponential calibration curve was obtained from the five (5) standards (Eqn 1). The sample spectra were plotted alongside

the spectrum of the DCS. The ratio of the sample spectra to the DCS spectrum was calculated and plotted. Linear estimates of suitable base lines were provided automatically by the acquisition programs. When base line drift was nonlinear, the data were discarded. The retention time at which this ratio was equal to 0.9 was selected as the critical retention time, RT, based on published method [39]. Then the critical peak molecular weight, M_P, was determined by plugging RT into the calibration curve. The critical Stokes radius, R_s, was determined from an empirical correlation for dextran (Eqn 2).

$$M_P = \alpha e^{BRT} \quad (\text{Eqn 1})$$

$$\text{Log } R_s = 0.470 \times \text{log } M_P - 1.513 \quad (\text{Eqn 2})$$

RESULTS

Surface morphology

HA/Alg hydrogel (Fig 3A) surface and cross-sections were imaged using SEM at 20X and 15x magnification, respectively. SEM images revealed a flat, dense and relatively featureless surface (Fig 3B). The bottom surface of the sheet had shallow circular indentations ranging from 2 to 10 µm in diameter. The cross-section revealed a lamellar structure (Fig 3C).

Confocal microscopy was performed on HA/Alg hydrogels labeled with alginate fluorescein and HA-rhodamine. HA (red) is observed as uniformly distributed in the Alg (green) matrix (Fig 3D).

Permeability

Gel permeation chromatography (GPC) spectra of the dextran challenge solution (DCS) and the dextran standards were obtained (Fig 4). The DCS chromatogram was broad and multimodal which was expected for a mixture of technical grade dextrans. The spectra of each dextran standard was narrow and spanned the range of molecular weights comprising the DCS. The peak at retention time of 17 minutes was observed in all dextran standards as well as the DCS solution, however this peak was absent in the baseline chromatogram (HPLC grade water). This peak can be assigned to an unknown impurity in dextran but was used as a reference to align spectra that were linearly shifted. A GPC calibration curve was prepared by plotting the peak retention time of each standard against the log of that standard's peak molecular weight. The calibration curve on a semi-log scale was linear with R² = 0.988 (Fig 5).

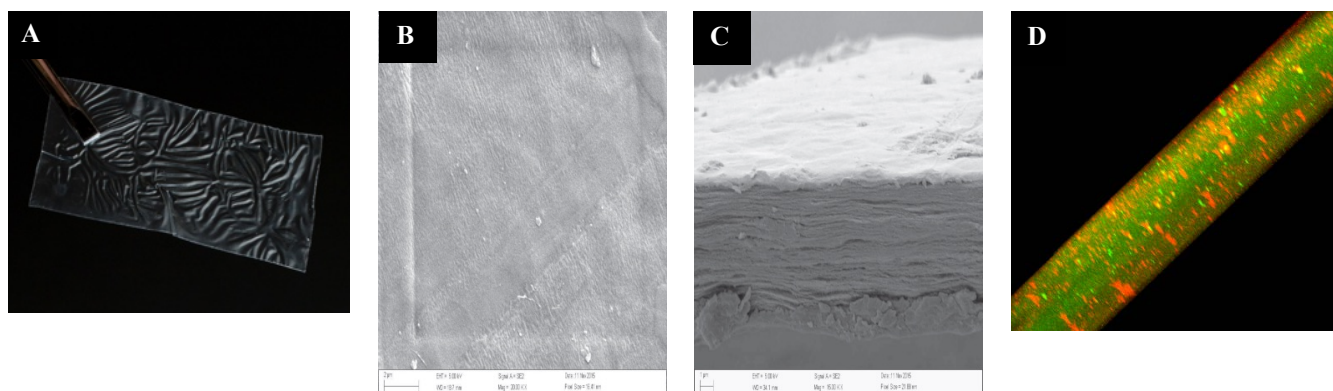


Fig 3. (A) HA/Alg hydrogel, (B) SEM image of the top surface at 20 X, (C) SEM image of cross-section surface at 15 X, (D) Confocal laser microscopy image of the hydrogel cross-section at 60X (green is Alg and red is HA)

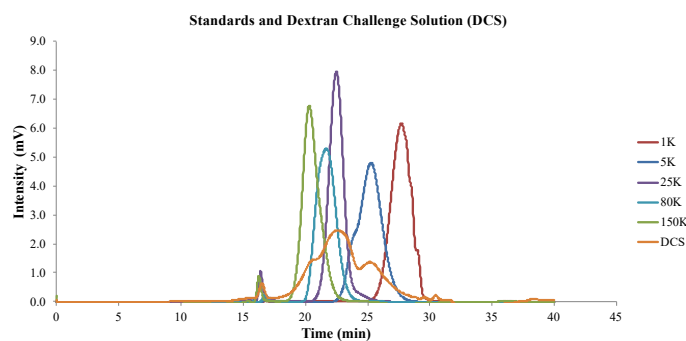


Fig 4. GPC spectra of the dextran standards and the dextran challenge solution (DCS)

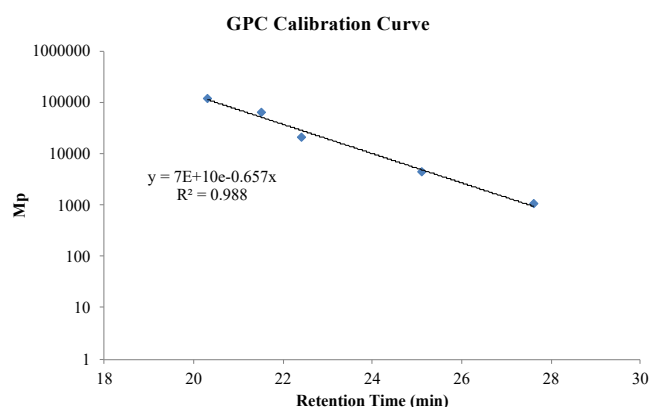


Fig 5. The GPC calibration curve obtained from dextran standards

DSC solution was collected from the donor compartment of the Franz diffusion cell at different timepoints (1.5, 6, and 24 hours) and analyzed using GPC (Fig 6). Chromatogram of samples collected at the 24 hr timepoint was shifted to a higher retention time and can be attributed to high dextran concentration in the DSC solution.

The intensity of the peak at 25.8 min in the DCS spectra (Fig 6), corresponding to low molecular weight dextrans (5 KDa) reduced over time and were negligible at 24 hrs. Dextrans with

molecular weight less than 5 kDa rapidly permeated through the HA/Alg hydrogel.

At 20.5 min the spectra of DCS at $t = 0$ and at $t = 6$ hrs began to diverge (Fig 7), corresponding to the maximum size dextrans that are capable of permeating through the hydrogel within 6 hrs. At 22.6 mins the intensity of the 6 hr spectrum is 90% that of the DCS spectrum at $t = 0$; therefore, this dataset was defined as the retention time corresponding to the molecular weight cut off (MWCO) of the membrane (Fig 8). The MWCO, 24,663 Da, was determined from the GPC calibration curve (Fig 6). The corresponding Stokes radius, 3.6 nm, was calculated from Eqn. 2. For macromolecules, the relationship between permeability (P) and Stokes radius (R_s) follow an exponential decline compared to small molecules where P decreases linearly with R_s .

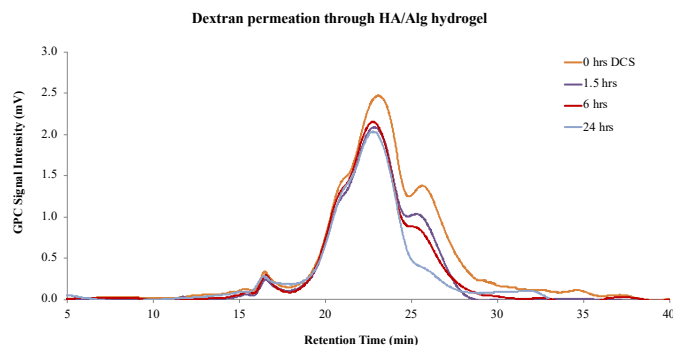


Fig 7. GPC spectra of the permeation at timepoint 0 and 6 h

The MWCO value cannot be directly used to assess which biomolecules can permeate the HA/Alg hydrogel. Solvated proteins and other macromolecules with equivalent molecular weight can have dramatically different conformation and diffusion rates; therefore, the hydrodynamic radius more closely reflects the apparent size adopted by the solvated, tumbling molecule. The Stokes radius (R_s) or hydrodynamic radius (R_h), is defined as the radius of an equivalent hard sphere diffusing at the same rate as the molecule under observation. The purpose of computing the Stokes radius from the MWCO was to allow the dextran permeation results to be generalized to macromolecules with

chemical compositions differing from dextran (Table 4). It is reasonable to compare Stokes radius calculated for the dextran MWCO from this permeation study with that of proteins and other biomolecules to assess their permeability through the hydrogel.

Table 4. The dextran permeation parameters

Parameter	MWCO	Max
Retention Time, RT (min)	22.616	20.483
Molecular Weight, MP (Da)	24,663	100,151
Stokes Radius, Rs (nm)	3.6	7.0

Fig 6. GPC spectra of the dextran challenge solution at timepoint 0, 1.5, 6, and 24 h

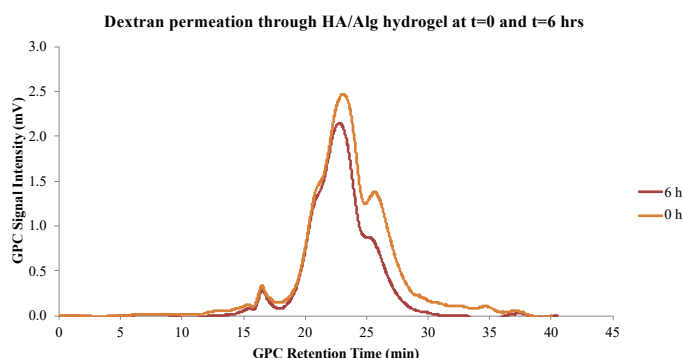


Fig 7. GPC spectra of the permeation at timepoint 0 and 6 hrs

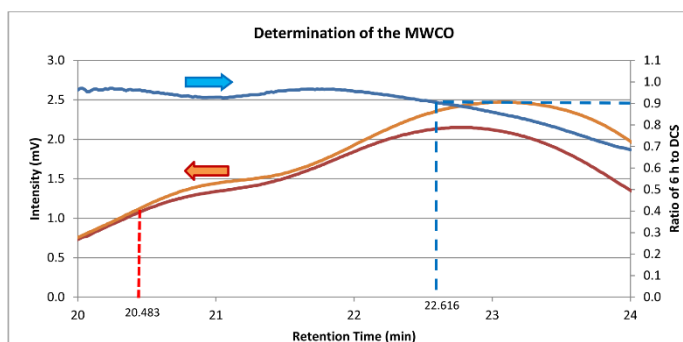


Fig 8. Determination of the molecular weight cutoff (MWCO) of HA/Alg hydrogel

DISCUSSION

Surface Morphology and Molecular Structure

The HA/Alg hydrogel is ultrathin and translucent (Fig 3A). The SEM images of the hydrogel surface suggest a dense and featureless morphology (Fig 3B, C). The confocal microscopy image of an HA/Alg hydrogel demonstrates that distribution of HA is homogenous within an Alg framework (Fig 3D). While the

hydrogel may not appear microscopically porous, microchannels of water allow rapid exchange and transport of nutrients and growth factors. These microchannels may support tissue repair and healing [40].

HA/Alg Hydrogel Permeability - Size

Hydrogels, in general, confer advantages as small molecule delivery vehicles as a result of high-water content and responsiveness to stimuli like pH or temperature. Diffusion of small proteins through alginate-based hydrogels is rapid as a result of the inherent porosity and hydrophilicity [41]. Encasing a healing nerve with a hydrogel may protect healing tissues while trapping and collecting fibrin, and providing a rudimentary scaffold for cellular migration during nerve regeneration [42]. While protein deposition or cellular attachment onto its surface is not likely, an HA/Alg hydrogel is permeable to small molecules such as growth factors, drugs, oxygen, potassium, calcium and other nutrients responsible for supporting nerve healing and regeneration (Table 5). The diffusion results in the present study suggest that molecules smaller than 24,663 Da, or a 3.6 nm Stokes radius, can readily permeate the HA/Alg hydrogel. Molecules with up to 7.0 nm Stokes radius may permeate the membrane over longer time periods (Fig 8, Table 4). These values align with published values, suggesting that alginate hydrogels are nanoporous (pore size ~ 5 nm) [43], thus allowing rapid diffusion of small molecules through the hydrogel.

The present study suggests that an HA/Alg hydrogel demonstrates the behavior of a semipermeable membrane, limiting permeable molecules by its pore size (~3.6-7 nm). Fibroblasts and collagenous proteins responsible for scar tissue formation may be blocked from reaching the injury site because they are too large to permeate the HA/Alg hydrogel (Fig 9).

Table 5. Literature reported values of Stokes/hydrodynamic radius of macromolecules that support nerve healing

Molecules that support nerve regeneration	Stokes/hydrodynamic radius (nm) from Literature	Ref.
Nerve Growth Factors (NGF)	6.6-7.6	[44]
Insulin-like Growth Factors (IGF)	1.54	[45]
Vascular Endothelial Growth Factor (VEGF)	3.02	[46]
Basic Fibroblast Growth Factor (bFGF)	2.28 – 2.8	‡ *
Brain derived Neurotrophic factor (BDNF)	2.75	*
Schwann cells	3.91-5.14	[47]
Transforming growth factor beta (TGFβ1) (from proteins of similar molecular weight)	2.8-3.5	[48]
Immunoglobulin G (IgG)	6.4	[49]
Hydrated Calcium ions (Ca ²⁺)	0.334	[50]
Hydrated potassium ions (K ⁺)	0.36-0.44	[51]
* Calculated using formula for globular molecules by Venturoli and Rippe [52] $a_e = 0.483 \times (MW)^{0.386}$		
‡ http://atlasgeneticsoncology.org/Genes/GC_FGF2.html		

HA/Alg Hydrogel Permeability – Kinetics

The permeability of an HA/Alg hydrogel was assessed for molecule size, however dextran does not readily bind to either

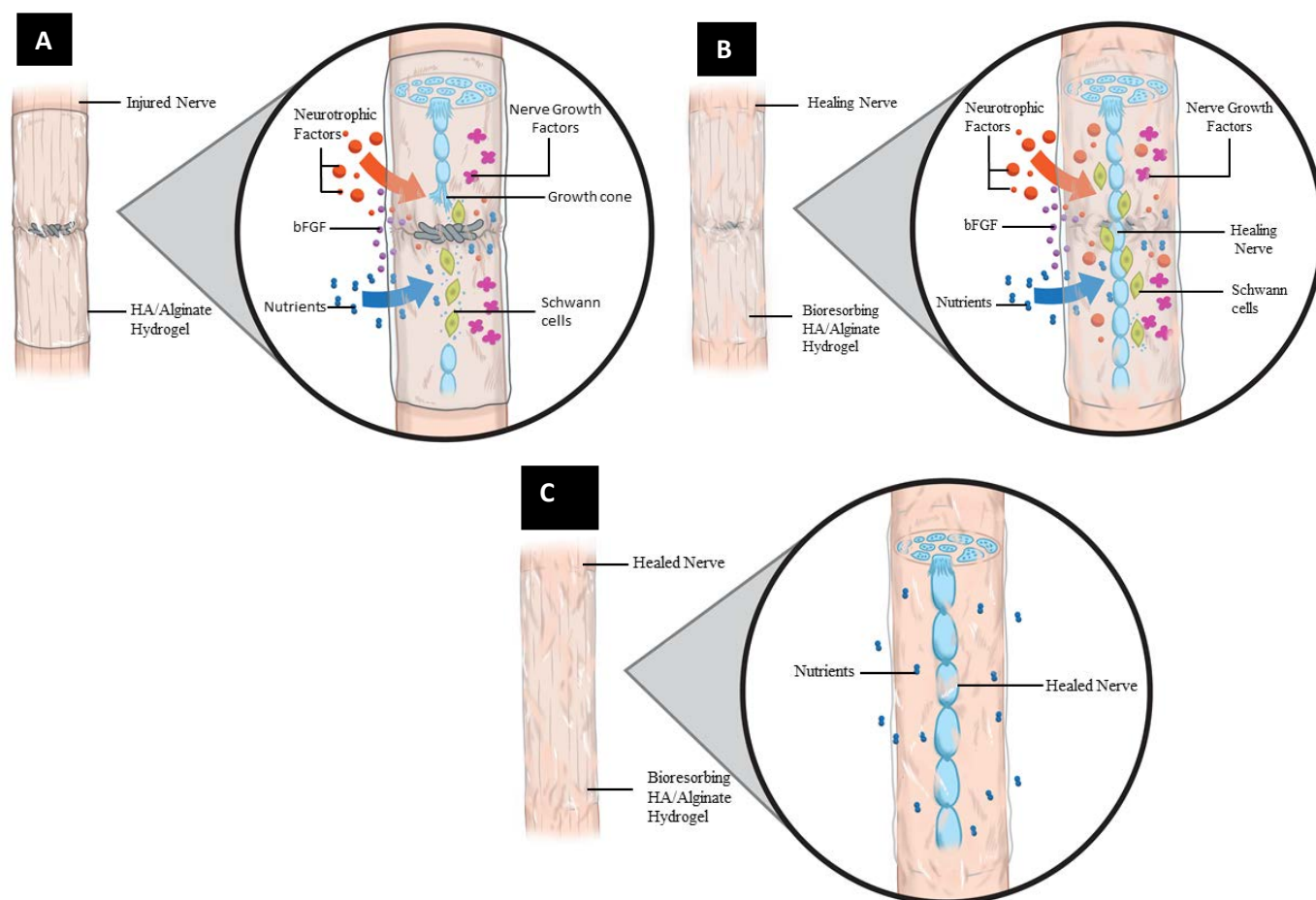


Fig 9. Schematic representation of an HA/Alg hydrogel wrapped around a peripheral nerve repair. A) HA/Alg hydrogel layer is permeable to small molecules and growth factors involved in the initial stages of healing and regeneration; B) late stages of healing protected minimally, allowing large molecules to reach the healed tissues; C) Healed nerve, protected minimally allowing normal exchange of nutrients.

alginate or hyaluronic acid. Additional molecular restriction beyond size may contribute to the overall permeability of an HA/Alg hydrogel. Research suggests that heparin-binding growth factors such as vascular endothelial growth factor (VEGF) or basic fibroblast growth factor (bFGF) exhibit reversible binding to alginate hydrogels, enabling a sustained and localized release [41, 53, 54]. This binding occurs via ionic interaction with negatively charged carboxylate groups on the alginate sugar rings.

HA/Alg Hydrogel Permeability - Bioresorption

The permeability of an HA/Alg hydrogel was assessed in a Franz diffusion chamber, void of the dynamic biological environment of healing peripheral nerve that contributes to hydrogel bioresorption. Bioresorption will inherently shift permeability as resorption of the hydrogel exposes underlying healing tissues to surrounding tissues (Fig 10). Therefore, the bioresorption timing has a significant role in managing at what point in the healing process larger molecules and cells can reach the injury site. An ideal nerve protector bioresorption rate has a half-life of 2-3 weeks following implantation [55]. An HA/Alg-blended hydrogel is

implanted as a hydrophilic layer of entangled biopolymers. These biopolymers begin to disentangle in the first few days following implantation [56]. As the polymers disentangle, the HA component is released, providing anti-inflammatory benefits in the early healing period [57-59]. Ongoing fluid turnover and physical movement allows the biopolymers to disentangle further and, thus, be exposed to bodily fluid and resorb via metabolic and hydrolytic activity over a two-year period [60]. The layer-by-layer resorption profile provides protection from large proteins and cells associated with formation of scar tissue primarily during the early stages of healing. It is important to note that the hydrogel is not replaced as cells do not adhere to or deposit onto its surface during bioresorption; thus once the hydrogel bioresorbs there is no longer an interface between the nerve and surrounding tissues, allowing desired larger molecules to reach the injury site during late stage healing (Fig 9).

CONCLUSIONS

HA/Alg hydrogels appear microscopically featureless on the surface and cross-sectionally lamellar and are nano-porous.

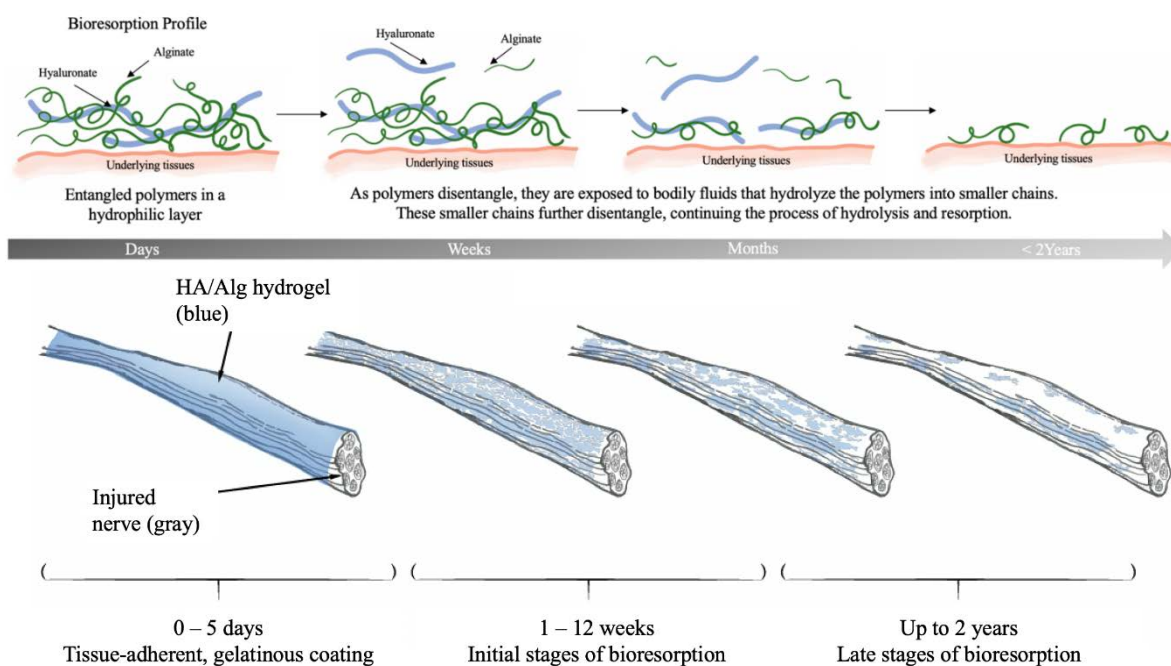


Fig 10. An HA/Alg hydrogel bioresorbs layer-by-layer throughout the healing period, up to two (2) years. Permeability increases with bioresorption. Entangled biopolymers disentangle in the first few days following implantation. Ongoing fluid turnover and physical movement allows the biopolymers to further disentangle and resorb via metabolic and hydrolytic activity. This cycle continues until all biopolymers are resorbed.

Migration of biomolecules through the hydrogel occurs via passive diffusion. Additionally, the large volume of water immobilized within the hydrogel allows for rapid exchange of oxygen and nutrients. In a permeability benchtop study using a standard Franz diffusion chamber, the HA/Alg hydrogel is easily permeable to dextran molecules correlating to macromolecules of 3.6 nm Stokes radius on a timescale (~ 6 hr) physiologically relevant to nerve healing. In this static setup, molecules up to 7.0 nm Stokes radius permeate over longer time periods. However, the dynamic environment of healing peripheral nerve allows for bioresorption of the hydrogel, inherently increasing permeability. This bioresorption occurs over a timescale relevant to nerve healing. HA/Alg hydrogels are permeable to small molecules such as oxygen, nutrients, water soluble drugs and growth factors required to support nerve healing and regeneration while large molecules, proteins, and cells such as fibroblasts are too large to have significant diffusion during the initial healing stages. Therefore, HA/Alg hydrogels are semipermeable to allow small molecules but prevent large molecules from reaching the injury site until early-stage healing is complete. This protection provides an optimal microenvironment for healing nerve by reducing the invasion of scar tissue forming fibroblasts to the injury site until late-stage healing.

REFERENCES

[1] C.R. Carvalho, J.M. Oliveira, R.L. Reis, (2019) Modern Trends for Peripheral Nerve Repair and Regeneration: Beyond the Hollow Nerve Guidance Conduit, *Frontiers in Bioengineering and Biotechnology* 7(337).

[2] C.R. Carvalho, R.L. Reis, J.M. Oliveira, 2020 Fundamentals and Current Strategies for Peripheral Nerve Repair and Regeneration, in: H.J. Chun, R.L. Reis,

A. Motta, G. Khang (Eds.), *Bioinspired Biomaterials: Advances in Tissue Engineering and Regenerative Medicine*, Springer Singapore, Singapore, pp. 173-201.

[3] A. Fex Svenningsen, L.B. Dahlin, (2013) Repair of the Peripheral Nerve-Remyelination that Works, *Brain Sci* 3(3) 1182-1197.

[4] B.J.F. Wong, R.L. Crumley, (1995) Nerve Wound Healing: An Overview*, *Otolaryngologic Clinics of North America* 28(5) 881-895.

[5] A.B. Dagum, (1998) Peripheral nerve regeneration, repair, and grafting, *J Hand Ther* 11(2) 111-7.

[6] J.K. Boyles, C.D. Zoellner, L.J. Anderson, L.M. Kosik, R.E. Pitas, K.H. Weisgraber, D.Y. Hui, R.W. Mahley, P.J. Gebicke-Haerter, M.J. Ignatius, et al., (1989) A role for apolipoprotein E, apolipoprotein A-I, and low density lipoprotein receptors in cholesterol transport during regeneration and remyelination of the rat sciatic nerve, *J Clin Invest* 83(3) 1015-31.

[7] M.J. Ignatius, E.M. Shooter, R.E. Pitas, R.W. Mahley, (1987) Lipoprotein uptake by neuronal growth cones in vitro, *Science* 236(4804) 959-62.

[8] K.R. Jessen, R. Mirsky, (2005) The origin and development of glial cells in peripheral nerves, *Nat Rev Neurosci* 6(9) 671-82.

[9] K.R. Jessen, R. Mirsky, A.C. Lloyd, (2015) Schwann Cells: Development and Role in Nerve Repair, *Cold Spring Harb Perspect Biol* 7(7) a020487.

[10] K. Hirata, M. Kawabuchi, (2002) Myelin phagocytosis by macrophages and nonmacrophages during Wallerian degeneration, *Microsc Res Tech* 57(6) 541-7.

[11] K.R. Jessen, R. Mirsky, (2016) The repair Schwann cell and its function in regenerating nerves, *J Physiol* 594(13) 3521-31.

[12] 21 CFR 882.5275.

[13] M. Szekalska, A. Pucilońska, E. Szymańska, P. Ciosek, K. Winnicka, (2016) Alginate: Current Use and Future Perspectives in Pharmaceutical and Biomedical Applications, *International Journal of Polymer Science* 2016 7697031.

[14] B.A. Aderibigbe, B. Buyana, (2018) Alginate in Wound Dressings, *Pharmaceutics* 10(2) 42.

[15] S.G. Kim, K.Y. Song, H.H. Lee, E.Y. Kim, J.H. Lee, H.M. Jeon, K.H. Jeon, H.M. Jin, D.J. Kim, W. Kim, H.M. Yoo, J.G. Kim, C.H. Park, (2019) Efficacy of an antiadhesive agent for the prevention of intra-abdominal adhesions after radical gastrectomy: A prospective randomized, multicenter trial, *Medicine (Baltimore)* 98(19) e15141-e15141.

[16] W. Manuskiatti, H.I. Maibach, (1996) Hyaluronic acid and skin: wound healing and aging, *Int J Dermatol* 35(8) 539-44.

- [17] W.Y. Chen, G. Abatangelo, (1999) Functions of hyaluronan in wound repair, *Wound Repair Regen* 7(2) 79-89.
- [18] P. Prang, R. Müller, A. Eljaouhari, K. Heckmann, W. Kunz, T. Weber, C. Faber, M. Vroemen, U. Bogdahn, N. Weidner, (2006) The promotion of oriented axonal regrowth in the injured spinal cord by alginate-based anisotropic capillary hydrogels, *Biomaterials* 27(19) 3560-9.
- [19] T. Hashimoto, Y. Suzuki, K. Suzuki, T. Nakashima, M. Tanihara, C. Ide, (2005) Review: peripheral nerve regeneration using non-tubular alginate gel crosslinked with covalent bonds, *J Mater Sci Mater Med* 16(6) 503-9.
- [20] K. Kataoka, Y. Suzuki, M. Kitada, T. Hashimoto, H. Chou, H. Bai, M. Ohta, S. Wu, K. Suzuki, C. Ide, (2004) Alginate enhances elongation of early regenerating axons in spinal cord of young rats, *Tissue Eng* 10(3-4) 493-504.
- [21] K. Suzuki, Y. Suzuki, M. Tanihara, K. Ohnishi, T. Hashimoto, K. Endo, Y. Nishimura, (2000) Reconstruction of rat peripheral nerve gap without sutures using freeze-dried alginate gel, *J Biomed Mater Res* 49(4) 528-33.
- [22] X. Li, T. Liu, K. Song, L. Yao, D. Ge, C. Bao, X. Ma, Z. Cui, (2006) Culture of neural stem cells in calcium alginate beads, *Biotechnol Prog* 22(6) 1683-9.
- [23] M. Mori, M. Yamaguchi, S. Sumitomo, Y. Takai, (2004) Hyaluronan-based Biomaterials in Tissue Engineering, *Acta Histochemica et Cytochemica* 37(1) 1-5.
- [24] T.C. Laurent, U.B. Laurent, J.R. Fraser, (1996) The structure and function of hyaluronan: An overview, *Immunol Cell Biol* 74(2) A1-7.
- [25] C. Costa, R. Tortosa, A. Domènech, E. Vidal, M. Pumarola, A. Bassols, (2007) Mapping of aggrecan, hyaluronic acid, heparan sulphate proteoglycans and aquaporin 4 in the central nervous system of the mouse, *J Chem Neuroanat* 33(3) 111-23.
- [26] W.M. Tian, S.P. Hou, J. Ma, C.L. Zhang, Q.Y. Xu, I.S. Lee, H.D. Li, M. Spector, F.Z. Cui, (2005) Hyaluronic acid-poly-D-lysine-based three-dimensional hydrogel for traumatic brain injury, *Tissue Eng* 11(3-4) 513-25.
- [27] S. Hou, W. Tian, Q. Xu, F. Cui, J. Zhang, Q. Lu, C. Zhao, (2006) The enhancement of cell adherence and inducement of neurite outgrowth of dorsal root ganglia co-cultured with hyaluronic acid hydrogels modified with Nogo-66 receptor antagonist in vitro, *Neuroscience* 137(2) 519-29.
- [28] K. Ikeda, D. Yamauchi, N. Osamura, N. Hagiwara, K. Tomita, (2003) Hyaluronic acid prevents peripheral nerve adhesion, *Br J Plast Surg* 56 342-347.
- [29] L.S. Peck, E.P. Goldberg, 2000 Polymer Solutions and Films as Tissue-Protective and Barrier Adjuvants, in: G.S. diZerega (Ed.), *Peritoneal Surgery*, Springer New York, New York, NY, pp. 499-520.
- [30] K.K. Wang, I.R. Nemeth, B.R. Seckel, D.P. Chakalis-Haley, D.A. Swann, J.W. Kuo, D.J. Bryan, C.L. Cetrulo, Jr., (1998) Hyaluronic acid enhances peripheral nerve regeneration in vivo, *Microsurgery* 18(4) 270-5.
- [31] B.R. Seckel, D. Jones, K.J. Heckimian, K.K. Wang, D.P. Chakalis, P.D. Costas, (1995) Hyaluronic acid through a new injectable nerve guide delivery system enhances peripheral nerve regeneration in the rat, *J Neurosci Res* 40(3) 318-24.
- [32] S.M. Carella, M.; Fino, P.; and Onesti, M. G., (2013) An atypical case of Henoch-Shönlein purpura in a young patient: treatment of the skin lesions with hyaluronic acid-based dressings, *In Vivo* 27(1) 147-151.
- [33] K.L. Aya, R. Stern, (2014) Hyaluronan in wound healing: rediscovering a major player, *Wound Repair Regen* 22(5) 579-93.
- [34] Y. Luo, K.R. Kirker, G.D. Prestwich, (2000) Cross-linked hyaluronic acid hydrogel films: new biomaterials for drug delivery, *Journal of Controlled Release* 69(1) 169-184.
- [35] N. El Kechai, E. Mamelle, Y. Nguyen, N. Huang, V. Nicolas, P. Chaminade, S. Yen-Nicolaÿ, C. Gueutin, B. Granger, E. Ferrary, F. Agnely, A. Bochot, (2016) Hyaluronic acid liposomal gel sustains delivery of a corticoid to the inner ear, *J Control Release* 226 248-57.
- [36] D. Szarek, K. Marycz, P. Bednarz, P. Tabakow, W. Jarmundowicz, J. Laska, (2013) Influence of calcium alginate on peripheral nerve regeneration: in vivo study, *Biotechnol Appl Biochem* 60(6) 547-56.
- [37] D.M. Hariyadi, N. Islam, (2020) Current Status of Alginate in Drug Delivery, *Adv Pharmacol Pharm Sci* 2020 8886095-8886095.
- [38] A.F. Quigley, K.J. Bulluss, I.L.B. Kyrtziz, K. Gilmore, T. Mysore, K.S.U. Schirmer, E.L. Kennedy, M. O'Shea, Y.B. Truong, S.L. Edwards, G. Peeters, P. Herwig, J.M. Razal, T.E. Campbell, K.N. Lowes, M.J. Higgins, S.E. Moulton, M.A. Murphy, M.J. Cook, G.M. Clark, G.G. Wallace, R.M.I. Kapsa, (2013) Engineering a multimodal nerve conduit for repair of injured peripheral nerve, *Journal of Neural Engineering* 10(1) 016008.
- [39] G. Tkacik, S. Michaels, (1991) A Rejection Profile Test for Ultrafiltration Membranes & Devices, *Bio/Technology* 9(10) 941-946.
- [40] A.S. Hoffman, (2012) Hydrogels for biomedical applications, *Advanced Drug Delivery Reviews* 64 18-23.
- [41] K.Y. Lee, D.J. Mooney, (2012) Alginate: properties and biomedical applications, *Prog Polym Sci* 37(1) 106-126.
- [42] G. Lundborg, (2004) Nerve injury and repair : regeneration, reconstruction, and cortical remodeling.
- [43] T. Boontheekul, H.J. Kong, D.J. Mooney, (2005) Controlling alginate gel degradation utilizing partial oxidation and bimodal molecular weight distribution, *Biomaterials* 26(15) 2455-65.
- [44] N.V. Costrini, R.A. Bradshaw, (1979) Binding Characteristics and Apparent Molecular Size of Detergent-Solubilized Nerve Growth Factor Receptor of Sympathetic Ganglia, *Proceedings of the National Academy of Sciences of the United States of America* 76(7) 3242-3245.
- [45] J.V. Nauman, P.G. Campbell, F. Lanni, J.L. Anderson, (2007) Diffusion of insulin-like growth factor-I and ribonuclease through fibrin gels, *Biophys J* 92(12) 4444-50.
- [46] M.O. Stefanini, F.T.H. Wu, F. Mac Gabhann, A.S. Popel, (2008) A compartment model of VEGF distribution in blood, healthy and diseased tissues, *BMC Systems Biology* 2(1) 77.
- [47] P.S. DiStefano, E.M. Johnson, Jr., (1988) Nerve growth factor receptors on cultured rat Schwann cells, *J Neurosci* 8(1) 231-241.
- [48] J.D. McCall, C.-C. Lin, K.S. Anseth, (2011) Affinity peptides protect transforming growth factor beta during encapsulation in poly(ethylene glycol) hydrogels, *Biomacromolecules* 12(4) 1051-1057.
- [49] D. Karlsson, G. Zacchi, A. Axelsson, (2002) Electronic speckle pattern interferometry: a tool for determining diffusion and partition coefficients for proteins in gels, *Biotechnol Prog* 18(6) 1423-30.
- [50] J.P. Barger, P.F. Dillon, (2016) Near-membrane electric field calcium ion dehydration, *Cell Calcium* 60(6) 415-422.
- [51] H. Moldenhauer, I. Díaz-Franulic, F. González-Nilo, D. Naranjo, (2016) Effective pore size and radius of capture for K⁺ ions in K-channels, *Scientific Reports* 6(1) 19893.
- [52] D. Venturoli, B. Rippe, (2005) Ficoll and dextran vs. globular proteins as probes for testing glomerular permselectivity: effects of molecular size, shape, charge, and deformability, *American Journal of Physiology-Renal Physiology* 288(4) F605-F613.
- [53] K.Y. Lee, M.C. Peters, D.J. Mooney, (2003) Comparison of vascular endothelial growth factor and basic fibroblast growth factor on angiogenesis in SCID mice, *J Control Release* 87(1-3) 49-56.
- [54] E.A. Silva, D.J. Mooney, (2010) Effects of VEGF temporal and spatial presentation on angiogenesis, *Biomaterials* 31(6) 1235-41.
- [55] B.A. Harley, M.H. Spilker, J.W. Wu, K. Asano, H.P. Hsu, M. Spector, I.V. Yannas, (2004) Optimal Degradation Rate for Collagen Chambers Used for Regeneration of Peripheral Nerves over Long Gaps, *Cells Tissues Organs* 176(1-3) 153-65.
- [56] S.M. Mayes, J. Davis, J. Scott, V. Aguilar, S.A. Zawko, S. Swinnea, D.L. Peterson, J.G. Hardy, C.E. Schmidt, (2020) Polysaccharide-based films for the prevention of unwanted postoperative adhesions at biological interfaces, *Acta biomaterialia* 106 92-101.
- [57] J. Lee, A. Spicer, (2000) Review Hyaluronan: a multifunctional, megaDalton, stealth molecule, *Curr Opin Cell Biol*. 12 581-6.
- [58] R. Li, H. Liu, H. Huang, W. Bi, R. Yan, X. Tan, W. Wen, C. Wang, W. Song, Y. Zhang, F. Zhang, M. Hu, (2018) Chitosan conduit combined with hyaluronic acid prevent sciatic nerve scar in a rat model of peripheral nerve crush injury, *Mol Med Rep* 17(3) 4360-4368.
- [59] J.A. Burdick, G.D. Prestwich, (2011) Hyaluronic acid hydrogels for biomedical applications, *Adv Mater* 23(12) H41-56.
- [60] Data on file at Alafair Biosciences (TR-011).

AUTHOR INFORMATION

Vidhi Maheshwari, PhD is Director of Research and Development at Alafair Biosciences, Inc.

Daniel L. Peterson, MD is a neurosurgeon in Austin, TX and is Medical Director at Alafair Biosciences, Inc.

Sarah Mayes, PhD is Chief Scientific Officer and Co-founder of Alafair Biosciences, Inc. She invented the Alafair technology.